

# Change-in-Slope Optimal Partitioning Algorithm in a Finite-Size Parameter Space

Vincent Runge

Université Paris-Saclay, CNRS, Univ Evry,  
Laboratoire de Mathématiques et Modélisation d'Evry,  
91037, Evry-Courcouronnes, France\*

Marco Pascucci

Université Paris-Saclay, CNRS, Univ Evry,  
Laboratoire de Mathématiques et Modélisation d'Evry,  
91037, Evry-Courcouronnes, France

Nicolas Deschamps de Boishebert

Université Paris-Saclay, CNRS, Univ Evry,  
Laboratoire de Mathématiques et Modélisation d'Evry,  
91037, Evry-Courcouronnes, France

## Abstract

We consider the problem of detecting change-points in univariate time series by fitting a continuous piecewise linear signal using the residual sum of squares. Values of the inferred signal at slope breaks are restricted to a finite set of size  $m$ . Using this finite parameter space, we build a dynamic programming algorithm with a controlled time complexity of  $O(m^2n^2)$  for  $n$  data points. Some accelerating strategies can be used to reduce the constant before  $n^2$ . The adapted classic inequality-based pruning is outperformed by a simpler “channel” method on simulations. Besides, our finite parameter space setting allows an easy introduction of constraints on the inferred signal. For example, imposing a minimal angle between consecutive segment slopes provides robustness to model misspecification and outliers. We test our algorithm with an isotonic constraint on an antibiogram image analysis problem for which algorithmic efficiency is a cornerstone in the emerging context of mobile-health and embedded medical devices. For this application, a finite state approach can be a valid compromise.

Keywords: Multiple change-point detection, change in slope, pruned dynamic programming, isotonic constraint, unimodal constraint, robust inference

## 1 Introduction

Detecting change-points in time series is a long-standing problem in statistics that have been tackled in many different ways since the 1950s. Originally developed for quality control in manufacturing [25], it has spread to the most modern sciences such as genomics [14, 5], neuroscience [22, 7] or climate change [3, 35] among many others. Due to the wide range of possible modeling assumptions and problem settings, change-point detection remains today an active scientific field, especially challenging for large data [24].

---

\*E-mail: vincent.runge@univ-evry.fr

## 1.1 Change in Mean

Last decades, researchers have been principally focused on the change-in-mean problem, which consists in inferring a piecewise constant signal from the data. This multiple change-point problem deals with finding the location and the number of changes in a time series  $y_{1:n}$  of length  $n$ . Among the  $2^{n-1}$  possible change-point vectors, the problem requires to select one vector for which a criterion is minimized or close to the minimum. Algorithmic efficiency is then a central challenge in order to rapidly infer a good change-point vector candidate.

Binary segmentation (BS) is one of the best known algorithm [28, 29] for solving this problem. It returns an approximate solution in time  $O(n \log(n))$ . Many other approaches have been proposed: see [33] for a review and [9] for some comparisons. A well-known alternative method is to use a dynamic programming approach [4] called optimal partitioning (OP) [18], which returns the best change-point vector minimizing the criterion<sup>1</sup>. Its principle consists in finding the best last segment in consecutive truncated time series  $y_{1:t}$  for  $t$  from 1 to  $n$ . Time complexity of this algorithm is of order  $O(n^2)$  as for each  $y_{1:t}$  we test the  $t$  available positions (candidates) for potential best last change-point. In the rest of this paper we will focus on approaches using dynamic programming algorithms.

In recent years, pruning ideas were proposed to reduce the set of candidates to consider for each truncated time series  $y_{1:t}$ , so that the complexity of OP became comparable with BS in some simulation studies. Two main classes of pruning are available: inequality-based pruning implemented in the PELT algorithm [21] and functional pruning [26, 23] implemented in the FPOP algorithm. PELT is based on a recursion on the position of the last change and remains close to OP (only a conditional expression is added). PELT is efficient only when the number of change-points is proportional to data length. FPOP is based on a recursion on the value of the last segment parameter and is more difficult to code: we need to update a functional cost at any step, that is a continuous piecewise quadratic function (in Gaussian model). However, this strategy achieves the best possible pruning and the log-linear time complexity on many data-sets [23].

## 1.2 Change in Slope

All these algorithms were developed to solve the change-in-mean problem. The change-in-slope problem is much less studied, even though many applications need such models [35, 19, 30, 32]. This problem consists in fitting a continuous piecewise linear signal based on minimizing the residual sum of squares of each segment. A few approaches directly tackle this problem [2, 8]. The latter is based on an FPOP-like algorithm and introduces a functional cost parametrized by the continuous variable  $\phi$  being the inferred value of the last considered data. Using this cost, they derive a one-parametric functional update and eventually get a time complexity between  $O(n^2)$  and  $O(n^3)$  (see simulations in Subsection 5.2).

The guideline of our work was the construction of a simplified efficient algorithm for change-in-slope problem, capable of returning a close-to-optimal change-point vector in a controlled time complexity of order  $O(n^2)$ . Furthermore, we were also interested in the possibility to easily constrain the inference as for change-in-mean algorithm FPOP [15]. Our algorithm can restrict the inference to an increasing signal but also force a minimal angle value between consecutive segment slopes. This latter option provides robustness to model misspecification and outliers, which is a desired features for many applications.

Our algorithm, called *slopeOP*, is an original PELT-like OP algorithm for change-in-slope problem, based on a finite set (of size  $m$ ) of allowed values for the inferred signal at slope breaks,

---

<sup>1</sup>The problem can have many best change-point vectors with the same minimal value given a criterion. However, this multiple solution is an event of zero probability with real-valued time series.

which we called *states*. Given a time series  $y_{1:n}$  of size  $n$ , like OP, our algorithm searches for the best last change-point in  $y_{1:t}$  for  $t$  from 1 to  $n$ . But, differently from OP, it looks for it in a finite set of couples (state,time) of size  $m \times t$ , where the state is in the finite *states* set. Summing up for all states and for  $t$  from 1 to  $n$ , we get an overall running time of order  $O(m^2n^2)$ .

The use of states is not only a bypass for reducing running time and enforce constraints. This restricted inference is also the right level of complexity for some applications as for example in online beat detection, for which the musician only needs integer beat-per-minute information. Other applications in embedded or resource-limited systems require time efficiency. In this case, reducing the number of states is a possible trade-off between running time and precision, as we demonstrate with our application to antibiogram image analysis.

### 1.3 Parameter Estimation

The criterion to optimize contains a penalty that is linear in the number of change-points. It is classically set to  $2k\hat{\sigma}^2 \log(n)$  for change-in-mean problem [34, 31], with  $\hat{\sigma}^2$  the estimated noise variance and  $k$  the number of changes. For change-in-slope problem, theorems for a similar penalty have been given in asymptotic regime [36]. As variance estimation is needed, we proposed a robust estimator of the variance based on an adaptation to the difference estimator of Hall et al. [12]. We provide a wide simulation study, showing the importance of developing algorithms dedicated to changes in slope with continuity constraint. We highlight in particular the difficulty for setting the penalty value for small data size as this penalty also depends on the signal shape. The minimum angle constraint helps inferring a signal closer to the true one, even if we use a sub-optimal penalty value. The minimum-angle constraint can be safely used to remove outliers in most cases, if adapted to the expected signal smoothness.

### 1.4 Outline

The outline of this paper is as follows. Section 2 introduces the model and describes the optimal partitioning algorithm for changes in slope with a simple description of the continuity constraint. We also give the three proposed constrained inference modes: isotonic, unimodal and minimal angle. Pruning-like approaches for speeding up the algorithm are exposed in Section 3. Section 4 is dedicated to variance estimation of time series with slopes. In the simulation study in Section 5 we show the benefit of using the continuity hypothesis by measuring the mean squared error (MSE) between the true signal and the inferred one. We also search for the range of penalties minimizing the MSE for 4 different simulation scenarios. We then compare the efficiency of the two proposed pruning methods and also compare the time complexity with the FPOP-like challenging algorithm CPOP [8]. Eventually, we show how using the minimal-angle constraint enhances the robustness of the algorithm. In last Section 6 we apply our algorithm to an antibiogram image analysis problem to find a unique change-point. In this application where non-decreasing signals are expected, the use of a monotonicity constraint improves detection precision. In this example, although the true signal is not expected to have a finite number of states, the finite-state trade-off allows a sensible gain in time and still a good analysis precision. In the context of mobile-health applications and hardware with limited computing capacity, where efficiency is important, such a trade-off could be fundamental.

Our change-in-slope algorithms are available into an R package on CRAN called *slopeOP*<sup>2</sup> and on github<sup>3</sup>.

<sup>2</sup><https://CRAN.R-project.org/package=slopeOP>

<sup>3</sup><https://github.com/vrunge/slopeOP>

## 2 Change-in-slope Optimal Partitioning

### 2.1 Model and Cost Function

We define the set of states  $\mathcal{S}$  as a finite set of accessible real values for beginning and ending values in inferred segments. When we write  $s = s_{min}, \dots, s_{max}$ , the variable  $s$  goes through all the values of  $\mathcal{S}$  from the smallest one to the biggest one. For computational efficiency we recommend to have  $\#\mathcal{S} = m \ll n$  but this is not mandatory.

Data are generated by the model

$$Y_t = s_i + \frac{s_{i+1} - s_i}{\tau_{i+1} - \tau_i}(t - \tau_i) + \epsilon_t, \quad t = \tau_i + 1, \dots, \tau_{i+1}, \quad i = 0, \dots, k,$$

with  $0 = \tau_0 < \tau_1 < \dots < \tau_k < \tau_{k+1} = n$ ,  $s_0, \dots, s_{k+1} \in \mathcal{S}$  and  $\epsilon_t \sim \mathcal{N}(0, \sigma^2)$  identically and independently distributed (iid).

This modeling imposes to define the cost for fitting data  $y_{(\tau+1):t}$ ,  $\tau < t$ , with linear interpolation from value  $s_1 \in \mathcal{S}$  to value  $s_2 \in \mathcal{S}$  as a residual sum of squares:

$$\mathcal{C}(y_{(\tau+1):t}, s_1, s_2) = \sum_{i=\tau+1}^t \left( y_i - \left( s_1 + (s_2 - s_1) \frac{i - \tau}{t - \tau} \right) \right)^2. \quad (1)$$

The value  $s_1$  is “unseen” as the cost  $(y_\tau - s_1)^2$  obtained at index  $\tau$  is not present in the summation. Note that this cost function doesn’t use a minimisation as in PELT: we cannot guarantee that splitting a segment into two segments would result in a smaller overall cost. This property is at the core of the PELT pruning rule. However, this choice of cost function will give us a simple update rule including the continuity condition for consecutive segments.

### 2.2 Optimization Problem

The *slopeOP* problem consists in finding the optimal partitioning of a time series  $y_{1:n} = (y_1, \dots, y_n) \in \mathbb{R}^n$  of size  $n$  into  $k + 1$  consecutive segments  $(y_{\tau_i+1}, \dots, y_{\tau_{i+1}})$  optimizing a penalized risk

$$Q_n^{slope} = \min_{\substack{\tau = (\tau_1, \dots, \tau_k) \in \mathbb{N}^k \\ \tau_0 = 0, \tau_{k+1} = n \\ (s_0, \dots, s_{k+1}) \in \mathcal{S}^{k+2}}} \sum_{i=0}^k \{ \mathcal{C}(y_{(\tau_i+1):\tau_{i+1}}, s_i, s_{i+1}) + \beta \} - \beta, \quad (2)$$

where the states defined inside the cost function provide the continuity constraint between successive segments and  $\beta$  is a positive penalty. This penalty controls the amount of evidence we need to add a change: the greater this quantity, the less is  $k$ . We emphasise that  $k$  is an unknown quantity. The penalty value is often set to  $2\hat{\sigma}^2 \log(n)$  [34, 31, 36] with  $\hat{\sigma}^2$  an estimation of the variance  $\sigma^2$ .

### 2.3 Dynamic Programming Algorithm

To address the continuity constraint in an efficient algorithm we introduce the function

$$Q_t : \begin{cases} \mathcal{S} & \rightarrow \mathbb{R} \\ u & \mapsto Q_t(u), \end{cases}$$

which is the optimal penalized cost up to position  $t$  with the inferred value at this position equal to  $u$ . Our goal is then to update the set

$$\mathcal{Q}_t = \{Q_t(u), u = s_{min}, \dots, s_{max}\},$$

at any time step  $t \in \{1, \dots, n\}$ , where  $s_{min}$  and  $s_{max}$  are bounds that can be determined in a pre-processing step. We find the objective value  $Q_n^{slope}$  with the minimization  $Q_n^{slope} = \min_{s_{min} \leq u \leq s_{max}} \{Q_n(u)\}$ .

**Proposition 2.1.** *The update rule with continuity constraint takes the form*

$$Q_t(v) = \min_{0 \leq t' < t} \left( \min_{s_{min} \leq u \leq s_{max}} \{Q_{t'}(u) + \mathcal{C}(y_{(t'+1):t}, u, v) + \beta\} \right), \quad (3)$$

where the state  $u$  in  $Q_{t'}$  and the cost function including states realizes the continuity constraint. At the initial step we have  $Q_0(v) = -\beta$  for all  $v \in \mathcal{S}$ .

*Proof.* The update rule is obtained by direct computations (we write “vectors  $\tau$  and  $s$ ” to mean the constraints in (2)):

$$\begin{aligned} Q_t(v) &= \min_{\substack{\text{vectors } \tau \text{ and } s \\ \tau_{k+1}=t, s_{k+1}=v}} \sum_{i=0}^k \{ \mathcal{C}(y_{(\tau_i+1):\tau_{i+1}}, s_i, s_{i+1}) + \beta \} - \beta \\ &= \min_{\text{vectors } \tau \text{ and } s} \sum_{i=0}^{k-1} \{ \mathcal{C}(y_{(\tau_i+1):\tau_{i+1}}, s_i, s_{i+1}) + \beta \} - \beta + \mathcal{C}(y_{(\tau_k+1):t}, s_k, v) + \beta \\ &= \min_{\substack{0 \leq t' < t \\ s_{min} \leq u \leq s_{max}}} \min_{\substack{\text{vectors } \tau \text{ and } s \\ \tau_k=t', s_k=u}} \sum_{i=0}^{k-1} \{ \mathcal{C}(y_{(\tau_i+1):\tau_{i+1}}, s_i, s_{i+1}) + \beta \} - \beta + \mathcal{C}(y_{(t'+1):t}, u, v) + \beta \\ &= \min_{\substack{0 \leq t' < t \\ s_{min} \leq u \leq s_{max}}} (Q_{t'}(u) + \mathcal{C}(y_{(t'+1):t}, u, v) + \beta). \end{aligned}$$

□

The corresponding optimal partitioning algorithm based on (3) is given in Algorithm 1.

---

**Algorithm 1:** Change-in-slope Optimal Partitioning (slopeOP)

---

**Input:** data  $y_{1:n}$ , set of states  $\mathcal{S} = \{s_{min}, \dots, s_{max}\}$  and penalty  $\beta > 0$

- 1  $Q$  = matrix of size  $(n+1) \times m$
- 2  $cp$  = matrix of size  $n \times m$
- 3  $U$  = matrix of size  $n \times m$
- 4 **for**  $v = s_{min}$  to  $s_{max}$  **do**
- 5 |  $Q(0, v) \leftarrow -\beta$
- 6 **end**
- 7 **for**  $t = 1$  to  $n$  **do**
- 8 | **for**  $v = s_{min}$  to  $s_{max}$  **do**
- 9 | |  $Q(t, v) \leftarrow \min_{0 \leq t' < t} \left( \min_{s_{min} \leq u \leq s_{max}} \{Q_{t'}(u) + \mathcal{C}(y_{(t'+1):t}, u, v) + \beta\} \right)$
- 10 | |  $cp(t, v) \leftarrow \operatorname{argmin}_{0 \leq t' < t} \left( \min_{s_{min} \leq u \leq s_{max}} \{Q_{t'}(u) + \mathcal{C}(y_{(t'+1):t}, u, v) + \beta\} \right)$
- 11 | |  $U(t, v) \leftarrow \operatorname{argmin}_{s_{min} \leq u \leq s_{max}} \left( \min_{0 \leq t' < t} \{Q_{t'}(u) + \mathcal{C}(y_{(t'+1):t}, u, v) + \beta\} \right)$
- 12 | **end**
- 13 **end**
- 14 **return**  $cp, U$  and  $Q(n, \cdot)$

---

The backtracking step is a little different from the standard optimal partitioning algorithm as we need to take into account the states.

---

**Algorithm 2:** Backtracking Algorithm

---

**Input:** Output of Algorithm 1 :  $cp, U$  and  $\{Q(n, v), v \in \mathcal{S}\}$

- 1  $chpts \leftarrow ()$
- 2  $states \leftarrow (\operatorname{argmin}_{s_{min} \leq v \leq s_{max}} \{Q(n, v)\})$
- 3  $t \leftarrow n$
- 4 **while**  $t > 0$  **do**
- 5      $chpts \leftarrow (t, chpts)$
- 6      $states \leftarrow (U(t, states(0)), states)$
- 7      $t \leftarrow cp(t, states(1))$
- 8 **end**
- 9 **return**  $chpts$  and  $states$

---

## 2.4 Inference with Constraints

Besides its unambiguous computational time efficiency in  $O(m^2n^2)$ , one of the benefit of this finite-state approach is the possibility to simply enforce some constraints in the inference. The quantity to optimize is then

$$Q_n^{ctt} = \min_{\substack{\text{vectors } \tau \text{ and } s \\ (\tau, s) \in U_{k+1}}} \sum_{i=0}^k \{\mathcal{C}(y_{(\tau_i+1):\tau_{i+1}}, s_i, s_{i+1}) + \beta\} - \beta, \quad (4)$$

where  $U_{k+1}$  is the set of constraints containing the positions (couples) that can be used in the minimization. We use notation  $\nu_i$  for a couple  $(\tau_i, s_i)$  position-state,  $(\tau, s) = ((\tau', n), (s', v))$  is a sequence of couples with the last one being  $(n, v)$  and  $U_{k+1}^{(n, v)}$  is the set  $U_{k+1}$  of sequences of couples with a last couple equal to  $(n, v)$ . A dynamic programming algorithm solving exactly (4) can be build if in  $U_{k+1}^{(n, v)}$  the information over the path  $(\nu_1, \dots, \nu_k)$  can be conveyed alongside this path to the current  $\nu_k$  position. That is:

$$\begin{aligned} U_{k+1}^{(n, v)} &= \{(\tau, s) \mid (\tau', s') \in U_k^{\nu_k}, f(\nu_1, \dots, \nu_k, (n, v)) = 1\} \\ &= \{(\tau, s) \mid (\tau', s') \in U_k^{\nu_k}, g(M(\nu_k), \nu_k, (n, v)) = 1\}, \end{aligned}$$

with  $g: \mathbb{R} \times (\{0, \dots, n\} \times \mathcal{S})^2 \rightarrow \{0, 1\}$  a validity test associated to the constraint. Function  $f$  is reduced to  $g$ . The ‘‘memory’’ function  $M: \{0, \dots, n\} \times \mathcal{S} \rightarrow \mathbb{R}$  summarizes the information of the path  $(\nu_1, \dots, \nu_k)$  and is associated in practice to the cost  $Q_{t'}(u)$  of the update rule. If  $g$  equals to 0, the couple  $\nu_k = (t', u)$  can not be considered in the minimization.

With this definition for  $U_{k+1}$  we get the update rule:

$$Q_t^{ctt}(v) = \min_{\substack{\tilde{v}=(t', u) \in \{0, \dots, t-1\} \times \mathcal{S} \\ \nu=(t, v), g(M(\tilde{\nu}), \tilde{\nu}, \nu)=1}} \left( Q_{t'}(u) + \mathcal{C}(y_{(t'+1):t}, u, v) + \beta \right). \quad (5)$$

In this rule, the positions  $\tilde{\nu}$  of the minimization operator are taken into account according to the  $g$  function value depending only on the current couple  $\nu = (t, v)$  and past events memorized by function  $M(\cdot)$ . We illustrate this constraint approach by the examples of isotonic, unimodal and robust inferences.

**Isotonic case.** The update rule for isotonic constraint is:

$$Q_t^{iso}(v) = \min_{0 \leq t' < t} \left( \min_{s_{min} \leq u \leq v} \{Q_{t'}(u) + \mathcal{C}(y_{(t'+1):t}, u, v) + \beta\} \right), \quad (6)$$

which is close to (3) but with a constrained minimization for variable  $u$ . Here  $M(\tilde{\nu}) = 0$  for all  $\tilde{\nu}$  and  $g(0, \tilde{\nu}, \nu) = 1$  if and only if  $u \leq v$  for  $\tilde{\nu} = (t', u)$  and  $\nu = (t, v)$ . We illustrate the use of the isotonic constraint in Section 6 with an antibiogram image analysis problem.

**Unimodal case.**  $M(\tilde{\nu})$  is equal to 1 if at position  $\tilde{\nu} = (t', u)$  no decreasing segment has been yet inferred. Otherwise  $M(\tilde{\nu}) = 0$ .  $g(1, \cdot, \cdot) = 1$  and

$$g(0, \tilde{\nu} = (t', u), \nu = (t, v)) = \begin{cases} 0 & \text{if } u < v, \\ 1 & \text{if } u \geq v. \end{cases}$$

Value  $M(\nu)$  is determined just after setting  $Q(\nu) = Q_t(\nu)$  using the slope sign information on the segment  $(\tilde{\nu}, \nu)$ .

**Minimal angle case.**  $M(\tilde{\nu}) \in \mathbb{R}$  is the slope value of the last inferred segment at position  $\tilde{\nu}$ . Here the value  $g(M(\tilde{\nu}), \tilde{\nu}, \nu)$  computes the angle deviation in degree between slope  $M(\tilde{\nu})$  and slope formed by  $(\tilde{\nu}, \nu)$ . If the obtained value is less than a threshold we have  $g(M(\tilde{\nu}), \tilde{\nu}, \nu) = 0$  and  $g(M(\tilde{\nu}), \tilde{\nu}, \nu) = 1$  otherwise. With this constraint, we tend to be robust to outliers with the right level of smoothness (the threshold). We also hope to get some kind of robustness to model misspecification (see simulations in Subsection 5.3).

In the R package *slopeOP*, we also provide a method returning the best change-point vector with a given fixed number of segments.

### 3 Accelerating Strategies

As revealed by Algorithm 1 the double loop for variables  $t$  and  $s$  (lines 7 and 8) is time consuming. We first give a formula for a constant-time computation of cost (1). Then we propose two accelerating strategies aiming at reducing the set of values to consider for the search for minimum in matrix  $Q$ . The first one is a PELT-like method based on inequalities of type “ $Q_{t'}(u) + \mathcal{C}(y_{(t'+1):t}, u, v) > Q_t(v)$ ”. The second one considers direct comparisons between elements of the minimization in (3). We test the efficiency of those two accelerating rules on simulations in Subsection 5.2. As the constraints can force the choice of non-minimal elements in (5) these methods can only be implemented in non-constraint setting (at the exception of the isotonic constraint).

#### 3.1 Efficient Cost Computation

**Proposition 3.1.** *The cost function (1) can be computed in constant time with the formula*

$$\begin{aligned} \mathcal{C}(y_{(t'+1):t}, u, v) = & S_t^2 - S_{t'}^2 - \frac{2}{t-t'} \left( (ut - vt')(S_t^1 - S_{t'}^1) + (v-u)(S_t^+ - S_{t'}^+) \right) \\ & + \frac{v^2 - u^2}{2} + \frac{u^2 + uv + v^2}{3}(t-t') + \frac{(v-u)^2}{6(t-t')}, \end{aligned}$$

where  $t' < t \in \{0, \dots, n\}$ ,  $(u, v) \in \mathcal{S}^2$  and

$$S_t^1 = \sum_{i=1}^t y_i, \quad S_t^2 = \sum_{i=1}^t y_i^2 \quad \text{and} \quad S_t^+ = \sum_{i=1}^t i y_i \quad \text{for all } t \in \{1, \dots, n\}.$$

The proof is straightforward by direct (tedious) calculations. The vectors  $(S_t^1)_{t=1,\dots,n}$ ,  $(S_t^2)_{t=1,\dots,n}$  and  $(S_t^+)_{t=1,\dots,n}$  are computed in a pre-processing step in  $O(n)$  time and saved. This is a marginal cost compared to the cost for Algorithm 1. Notice that the  $O(m^2n^2)$  time complexity is obtained using the result of Proposition 3.1.

### 3.2 Inequality-based Pruning

With the following Proposition 3.2 we build a standard inequality-based pruning that has the specificity to take into account future data. At each position  $v \in \mathcal{S}$ , we need to update a set of positions:

$$\mathcal{U}(t, v) \subset \{(t', u), t' \in \{0, \dots, t-1\}, u \in \{s_{min}, \dots, s_{max}\}\},$$

to get  $\mathcal{U}(t+1, v)$ . There are  $m$  such sets. Therefore, we actually chose to transfer information at constant state value.

**Proposition 3.2.** *At time  $t$  and position  $v$ , suppose that there exists  $t' < t$  and  $u \neq v$  such that*

$$Q_{t'}(u) + \mathcal{C}(y_{(t'+1):t}, u, v) > Q_t(v). \quad (7)$$

We define  $S_t^{t'} = \sum_{i=t'+1}^t (i-t')y_i$  and coefficients  $(\alpha_t^-, \alpha_t^+, \gamma_t^-, \gamma_t^+)$  such that

$$\alpha_t^+ T + \gamma_t^+ \leq \sum_{i=t'+1}^{T-1} y_i \frac{T-i}{T-t} \leq \alpha_t^- T + \gamma_t^-, \quad T = t+1, \dots, n.$$

We also define for all integers  $T > t$  the affine in  $T$  functions:

$$\begin{cases} f^+(T) = \left( \alpha_t^+ - \frac{u+2v}{6} \right) T + t' \frac{u+2v}{6} - \frac{v-u}{12(t-t')} + \frac{S_t^{t'}}{t-t'} + \gamma_t^+, \\ f^-(T) = \left( \alpha_t^- - \frac{u+2v}{6} \right) T + t' \frac{u+2v}{6} - \frac{v-u}{12(t-t')} + \frac{S_t^{t'}}{t-t'} + \gamma_t^-. \end{cases}$$

If  $f^+(t+1) \geq 0$  and  $f^+(n) \geq 0$  (case  $v-u > 0$ ) or if  $f^-(t+1) \leq 0$  and  $f^-(n) \leq 0$  (case  $v-u < 0$ ) then the position  $(t', u)$  doesn't have to be considered for further iterations  $T > t$  for computing  $Q_T(v)$  in Algorithm 1. We remove  $(t', u)$  from  $\mathcal{U}(T, v)$  for all  $T > t$ .

*Proof.* In order to prune we need to force the inequality

$$\mathcal{C}(y_{(t'+1):T}, u, v) \geq \mathcal{C}(y_{(t'+1):t}, u, v) + \mathcal{C}(y_{(t+1):T}, v, v),$$

to be true for all  $T \geq t+1$  and fixed  $t', t, u, v$ . Using the cost definition (1), the inequality is equivalent to

$$\begin{aligned} (v-u) \left( \sum_{i=t'+1}^t y_i \frac{(i-t')(T-t)}{(t-t')(T-t')} + \sum_{i=t'+1}^{T-1} y_i \frac{T-i}{T-t'} \right) \\ \geq (v-u)(T-t) \left( \frac{u+2v}{6} + \frac{v-u}{12(t-t')(T-t')} \right) \end{aligned}$$

and then

$$(v-u)g_t(T) \geq (v-u) \left( (T-t') \left( \frac{u+2v}{6} \right) + \frac{v-u}{12(t-t')} - \frac{S_t^{t'}}{t-t'} \right) \quad (8)$$

with

$$g_t(T) = \begin{cases} \sum_{i=t+1}^{T-1} y_i \frac{T-i}{T-t} & \text{for } T = t+2, \dots, n, \\ 0 & \text{for } T = t+1. \end{cases}$$

As the right hand side of inequality (8) is linear in  $T$  we choose the following strategy: find coefficients  $(\alpha_t^-, \alpha_t^+, \gamma_t^-, \gamma_t^+)$  of an upper and lower linear approximation such that

$$\alpha_t^+ T + \gamma_t^+ \leq g_t(T) \leq \alpha_t^- T + \gamma_t^-, \quad T = t+1, \dots, n.$$

We then introduce the linear-in- $T$  functions  $f^-$  and  $f^+$  defined in the Proposition. To prove that the inequality  $f^+(T) \geq 0$  holds for all  $T = t+1$  to  $n$  we only need to have  $f^+(t+1) \geq 0$  and  $f^+(n) \geq 0$  due to the linearity of  $f^+$ . With the same argument for  $f^-$  the result is proven.  $\square$

The use of additional parameters (the states) in cost function leads to a more complex pruning rule than the one for standard PELT [21] as the overall cost is not guaranteed to decrease as the number of change-point increases. However, in case  $u = v$  we have a simpler result:

**Proposition 3.3.** *At time  $t$ , if there exists  $t' \in \{0, \dots, t-1\}$  such that*

$$Q_{t'}(v) + \mathcal{C}(y_{(t'+1):t}, v, v) > Q_t(v), \quad (9)$$

*then the position  $t'$  doesn't have to be considered for further iterations  $T > t$  for computing  $Q_T(v)$  in Algorithm 1.*

*Proof.* We use the fact that we have

$$\mathcal{C}(y_{(t'+1):t}, v, v) + \mathcal{C}(y_{(t+1):T}, v, v) = \mathcal{C}(y_{(t'+1):T}, v, v),$$

for any  $t' < t < T$ . Adding the quantity  $\mathcal{C}(y_{(t+1):T}, v, v)$  to (9) and using this equality we get

$$Q_{t'}(v) + \mathcal{C}(y_{(t'+1):T}, v, v) + \beta > Q_t(v) + \mathcal{C}(y_{(t+1):T}, v, v) + \beta,$$

which means that  $(t', v)$  is a choice less optimal than  $(t, v)$  for the minimization in  $Q_T(v)$ .  $\square$

We have a second pruning rule for v-constant positions which is original in the sense that a recent position can be pruned by an older one.

**Proposition 3.4.** *At time  $t$ , if there exists  $t' \in \{0, \dots, t-1\}$  such that*

$$Q_{t'}(v) + \mathcal{C}(y_{(t'+1):t}, v, v) \leq Q_t(v), \quad (10)$$

*then the position  $t$  doesn't have to be considered for further iterations  $T > t$  for computing  $Q_T(v)$  in Algorithm 1.*

The proof is the same as for Proposition 3.3.

**Remark 3.1.** *One of the two inequalities (9) and (10) is always satisfied so that the subset  $\mathcal{U}(t, v) \cap \{(t', v), t' = 1, \dots, t-1\}$  contains at most one element.*

### 3.3 Channel Pruning

We propose a new rule for speeding-up the algorithm, called the “channel method”. It does not prune the position  $(t', u)$  in the classical sense, as a non-considered value can be further reintegrated in the minimization (in a set  $\mathcal{U}(t, v)$ ). However its simplicity could help to reduce time complexity.

We expect the cost  $Q$  to verify some structural properties. In particular,

$$q_t = \begin{cases} \mathcal{S} & \rightarrow \mathbb{R} \\ v & \mapsto Q_t(v) \end{cases}$$

should have a minimum for  $v$  “near” the data, which means that  $q_t$  is, for most  $t$ , decreasing until a state  $v_l$  and increasing from a state  $v_u \geq v_l$ . The function

$$C_{(t'+1):t}^{\tilde{v}} = \begin{cases} \mathcal{S} & \rightarrow \mathbb{R} \\ v & \mapsto \mathcal{C}(y_{(t'+1):t}, v, \tilde{v}) \end{cases}$$

has a global minimum that can be easily found (it’s a quadratic function). The idea is to study the variations of  $q_{t'} + C_{(t'+1):t}^{\tilde{v}}$  in order to leave out the state values for which we know they are away from the argminimum.

**Proposition 3.5.** *We consider the function  $q_{t'} + C_{(t'+1):t}^{\tilde{v}}$  with  $t' + 1 < t$ . The minimum of this function is inside the interval*

$$I_{t'}^{\tilde{v}} = \mathcal{S} \setminus (S_{min} \cup S_{max}),$$

with

$$\begin{cases} S_{min} = \{s_{min}, \dots, \min(v_l^{-1}, [v^*]^{-1})\}, \\ S_{max} = \{\max(v_u^{+1}, [v^*]^{+1}), \dots, s_{max}\}, \end{cases}$$

where  $[\cdot]$  is the nearest “value in set  $\mathcal{S}$ ” operator and  $(\cdot)^{+1}$  (resp.  $(\cdot)^{-1}$ ) denotes the following (resp. preceding) value in the ordered set  $\mathcal{S}$ . Function  $q_{t'}$  is decreasing on  $\{s_{min}, \dots, v_l\}$  and increasing on  $\{v_u, \dots, s_{max}\}$ . We also know that the argminimum of  $C_{(t'+1):t}^{\tilde{v}}$  is given by formula

$$v^* = \frac{6}{(t - t' - 1)(2(t - t') - 1)} \sum_{i=t'+1}^t \left[ (t - i)y_i \right] - \tilde{v} \frac{t - t' + 1}{2(t - t') - 1}.$$

*Proof.*  $v^*$  is easy to compute as the argminimum of the quadratic function  $C_{(t'+1):t}^{\tilde{v}}$ . The set  $S_{min}$  (resp.  $S_{max}$ ) corresponds to the set on which we know that function  $q_{t'} + C_{(t'+1):t}^{\tilde{v}}$  is decreasing (resp. increasing) with the next (resp. previous) value in  $\mathcal{S}$  giving a smaller output.  $\square$

Notice that the closest state search  $[v^*]$  is a  $O(1)$  operation if  $\mathcal{S}$  is made of consecutive integers or a  $O(\log(n))$  operation in a general ordered list. We define the matrix  $\mathcal{Q} \in \mathbb{R}^{m \times n}$  with  $Q_{ij} = Q_j(s_i)$ . The name “channel” comes from the fact that the matrix  $\mathcal{Q}$  is restricted by a channel with fixed  $v_u$  and  $v_l$  states for each column of this matrix. For all  $\mathcal{U}(t, v)$ , this channel is updated to  $I_{t'}^{\tilde{v}}$  after computing the value  $v^*$  and using Proposition 3.5.

## 4 Variance Estimation

With real data-sets the noise level  $\sigma^2$  in time series is an unknown quantity that has to be estimated. In change-in-mean problems there exist many estimators for the variance of a time-series as for example the mean absolute deviation (MAD) or HALL estimators [12]. They have

the property to be slightly sensitive to change-points when the number of changes is small compared to data length. In slope problems we face the additional difficulty to remove the slope effect. We suggest to adapt the HALL estimator to our change-in-slope problem. In classic mean problem, we have for HALL of order 3:

$$\hat{\sigma}_{mean}^2 = \frac{1}{n-3} \sum_{j=1}^{n-3} \left( \sum_{k=0}^3 d_k Y_{j+k} \right)^2,$$

with  $d_0 = 0.1942$ ,  $d_1 = 0.2809$ ,  $d_2 = 0.3832$  and  $d_3 = -0.8582$ . We apply Hall on the successive differences (“HALL Diff”):

$$\hat{\sigma}_{slope}^2 = \frac{1}{(n-4)\Delta} \sum_{j=1}^{n-4} \left( \sum_{k=0}^3 d_k (Y_{j+k+1} - Y_{j+k}) \right)^2,$$

with  $\Delta = d_0^2 + (d_1 - d_0)^2 + (d_2 - d_1)^2 + (d_3 - d_2)^2 + d_3^2 = 1.527507$  a normalization coefficient.

To evaluate the quality of the HALL Diff estimator, we simulate 100 time series of length 100 with 2 signals, one piecewise linear and the other sinusoidal as in Figure 1.

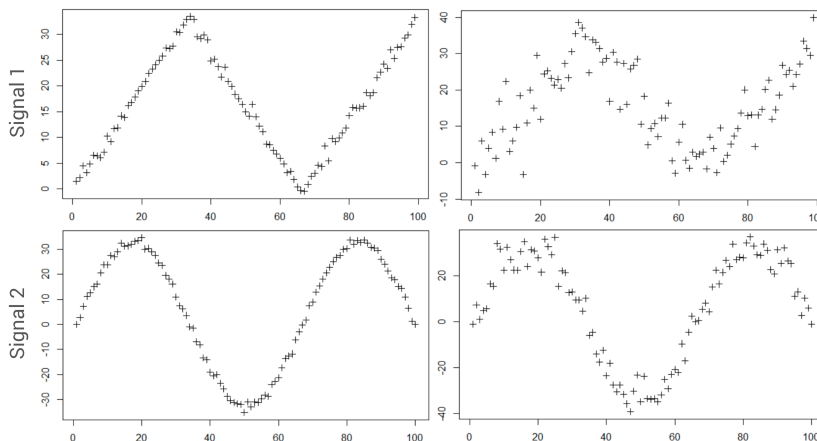


Figure 1: Examples for the linear and sinusoidal time series with noise  $\sigma = 1$  (left) and  $\sigma = 5$  (right).

In Table 4, we present results for estimating the standard deviation  $\sigma$  for 100 simulated time series for each level of noise ( $\sigma = 1, \dots, 5$ ). We easily conclude that the HALL Diff method gives very accurate results, even with a non-linear (sinusoidal) model. We also have a better precision of the estimated sigma for HALL Diff than for MAD.

## 5 Simulation Study

Our simulation study is split into three parts. We first compare the mean squared error (MSE) between the true signal and the inferred one with many different algorithms and study the impact of choosing different  $\beta$  penalty values. In the second part, we select our main competitor CPOP to challenge it in terms of computational efficiency. Finally, we consider misspecified time series with an heavy-tailed noise and explore the capacity of *slopeOP* with a minimal angle between segments to infer a good model on a range of penalties.

method	signal	$\sigma$	1	2	3	4	5
MAD	slope	mean( $\hat{\sigma}$ )	<b>1.21</b>	<b>2.12</b>	<b>3.08</b>	<b>4.04</b>	<b>5.10</b>
		sd.( $\hat{\sigma}$ )	0.13	0.23	0.37	0.45	0.68
	sinus	mean( $\hat{\sigma}$ )	<b>2.16</b>	<b>2.58</b>	<b>3.37</b>	<b>4.25</b>	<b>5.24</b>
		sd.( $\hat{\sigma}$ )	0.15	0.27	0.40	0.50	0.62
HALL	slope	mean( $\hat{\sigma}$ )	<b>1.84</b>	<b>2.51</b>	<b>3.37</b>	<b>4.31</b>	<b>5.28</b>
		sd.( $\hat{\sigma}$ )	0.047	0.12	0.22	0.26	0.37
	sinus	mean( $\hat{\sigma}$ )	<b>3.50</b>	<b>3.88</b>	<b>4.50</b>	<b>5.21</b>	<b>5.99</b>
		sd.( $\hat{\sigma}$ )	0.03	0.08	0.14	0.26	0.30
HALL Diff	slope	mean( $\hat{\sigma}$ )	<b>1.01</b>	<b>1.99</b>	<b>2.99</b>	<b>4.04</b>	<b>5.04</b>
		sd.( $\hat{\sigma}$ )	0.092	0.19	0.28	0.34	0.47
	sinus	mean( $\hat{\sigma}$ )	<b>1.02</b>	<b>1.98</b>	<b>3.00</b>	<b>3.97</b>	<b>4.98</b>
		sd.( $\hat{\sigma}$ )	0.09	0.17	0.24	0.35	0.41

Table 1: Variance estimation with MAD, HALL and HALL Diff estimators

## 5.1 MSE Competition with Other Algorithms

We consider the 5 following methods:

- OP-2D : we fit the data with the PELT algorithm but the cost function on a segment is the residual sum of squares between data and a linear regression (2-dimensional fit). In that case, we don't have any continuity constraint;
- FPOP : The standard efficient gaussian FPOP algorithm [23] used on differenced data  $z_t = y_{t+1} - y_t$ ,  $t = 1, \dots, n - 1$ . The continuity is obtained by construction;
- RFPOP : Same algorithm as the previous FPOP but with robust biweight loss (with robust parameter  $K = 3\sigma$ ) [10];
- CPOP : A FPOP-like algorithm for changes in slope with continuity constraint [8]. The set of states is here infinite-dimensional ( $\mathbb{R}$ ) and not finite as for *slopeOP*;
- slopeOP : Our finite-state change-in-slope OP algorithm.

The first idea to detect change in slope consists in looking at changes in data  $z_t = y_{t+1} - y_t$  with any well-known change-in-mean algorithm. We use here the efficient FPOP and robust FPOP algorithms for the inference. We highlight in Figure 2 the fact that with a simple hat-shaped model and a low level of noise, the FPOP algorithms give bad performances as the number of datapoint increases. Therefore, we left out these two methods and study only the behavior of three algorithms: OP-2D, CPOP and *slopeOP*.

We now consider 4 scenarios of increasing complexity with 3 levels of noise as shown in Figure 3. The beginning and ending values of all segments are integers in  $\{0, \dots, 60\}$  and we choose a set of states  $\mathcal{S} = \{-10, \dots, 70\}$  to reduce side effects in limit points (0 and 60). We simulate 30 time series of length 500 for each of the couple (scenario, noise) and draw the graph of the MSE (between the true signal and the inferred signal) with respect to  $b = \frac{\beta}{\sigma^2 \log(n)}$ , where  $\sigma$  is the chosen known level of noise. For each of the 30 time series, the 3 algorithms are run for  $b = 0.1, 0.2, \dots, 4.9, 5$  and each point of the MSE curve is the mean over the 30 independent simulations. For the smallest MSE in each of the 12 MSE curves, we present the 30 corresponding results in the boxplots. The last column shows the obtained segments for the best (smallest MSE) of the 30 results in boxplots (for OP-2D and *slopeOP*).

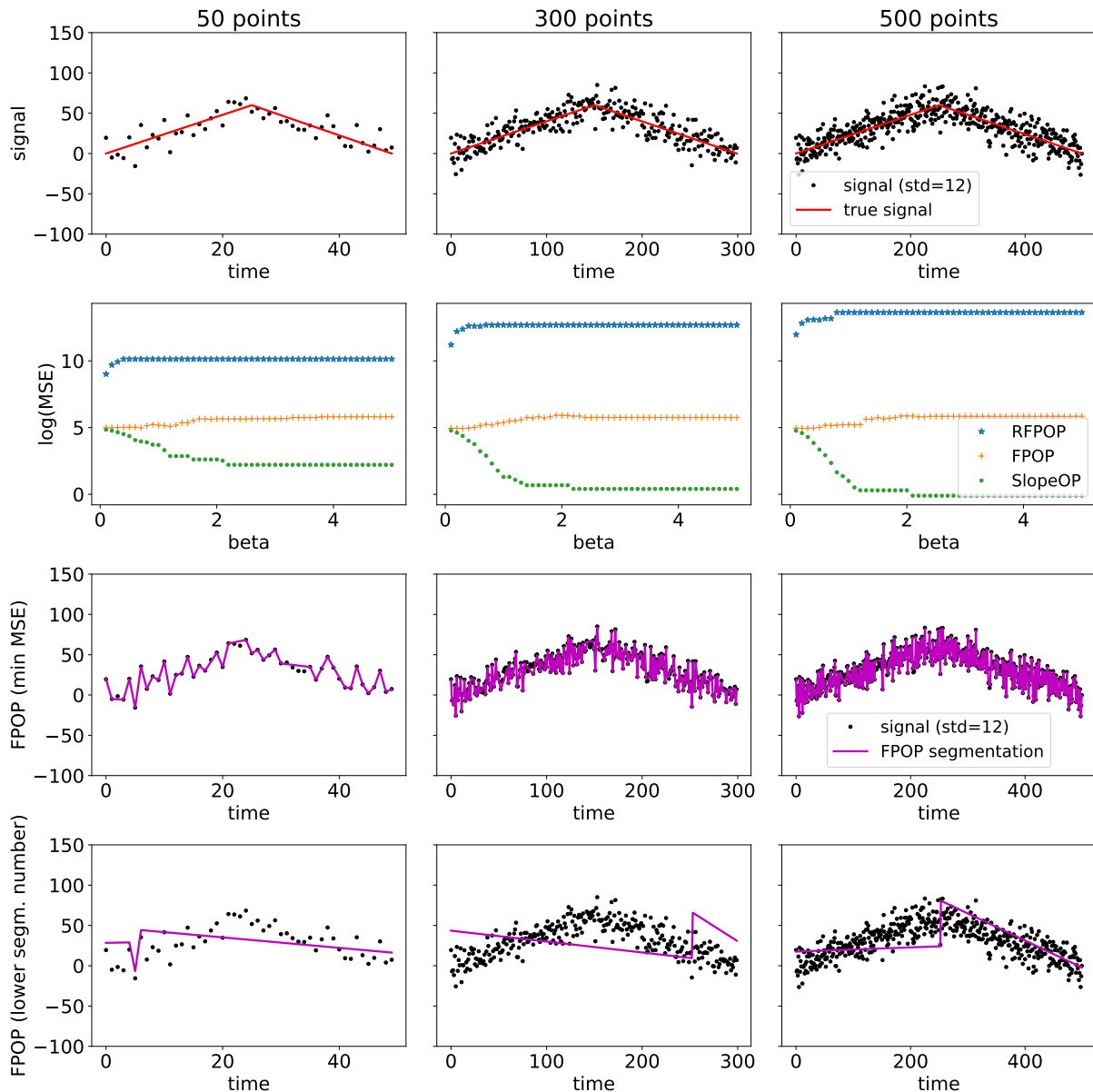


Figure 2: The first row presents 3 time-series of size 50, 300 and 500 that are obtained by the black hat-shaped signal with an additive Gaussian noise with  $\sigma = 12$ . For a range of values for  $b = \frac{\beta}{\sigma^2 \log(n)}$  we plot the average  $\log(\text{MSE})$  curve for algorithms FPOP, RFPOP and *slopeOP* for 10 simulated time series. The first two algorithms give performances far away from *slopeOP*. In the third row we show an example of an inferred signal by FPOP with a  $b$  value corresponding to the minimum in  $\log(\text{MSE})$  curves. In last row we plot the segments obtained by the biggest possible  $b$  value before having a unique segment with the same data. We observe that we fail to obtain only 2 segments and that we obviously obtain an unrealistic result.

We discuss the results for the intermediate level of noise ( $\sigma = 12$ ) exposed in Figure 4, other results are exposed in A. For all scenarios CPOP and *slopeOP* give very close and similar good results compared to OP-2D. The lack of continuity constraint explains the higher MSE value for OP-2D in scenarios 1, 3 and 4. For all scenarios and all noise levels, the optimal penalty in our simulations with  $n = 500$  is close to  $b = 2$  for *slopeOP* and CPOP as expected in asymptotic regime [36].

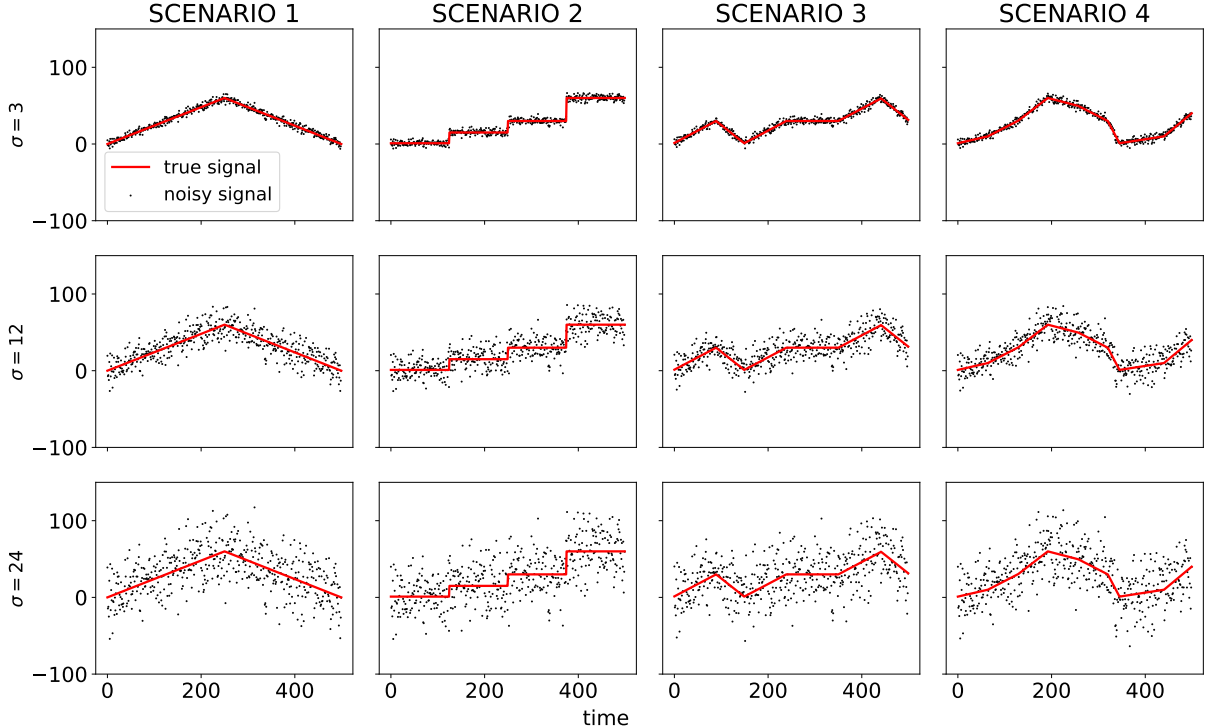


Figure 3: The plain black line is the true signal. For each scenario we simulate time series with an additive Gaussian noise of increasing standard deviation ( $\sigma = 3, \sigma = 12, \sigma = 24$ ). Each plot shows a realisation of this procedure with 500 data points. The number of segments for scenarios 1 to 4 is respectively 2, 7, 6 and 8.

## 5.2 Computational Efficiency

In this section we consider hat-shaped time series with a signal from 10 to 50 and 61 integers states ( $\mathcal{S} = \{0, \dots, 60\}$ ) for inference.

We first compare time efficiency for the two accelerating methods: channel-based rule and inequality-based pruning. In Figure 5 we easily understand that the channel rule is much more efficient for all level of noise. It may be possible to get similar pruning efficiency in some very particular situations but we conclude with these simulations that the default rule should always be the channel method.

We run the *slopeOP* and CPOP algorithms over 10 simulations for each  $n$  from  $n = 100$  to  $n = 1500$  by a step of size 10. In Figure 6, we plot the mean time for each algorithm and two levels of noise in log-log scale. The results confirms the quadratic complexity for *slopeOP* and a complexity for CPOP between  $n^2$  and  $n^3$  (closer to  $n^3$  with a higher level of noise). For example, with  $n = 1500$  and  $\sigma = 24$  we have a mean time of 43s for CPOP and 21s for *slopeOP*.

## 5.3 A Minimum Angle Between Consecutive Segments

We generate time series in scenario 1 of the hat-shaped signal with an heavy-tailed noise (a Student distribution with a degree of freedom equal to 3) with  $\sigma = 24$ . Simple computations give an angle of about  $153^\circ$  between the two segments. We choose to fix a minimal angle between segments to  $130^\circ$ . We explore the value of the MSE returned by the standard *slopeOP* algorithm compared with the same algorithm with smoothing option for a range of penalty values. We also return the number of inferred segments. Each data-point is the mean over 10

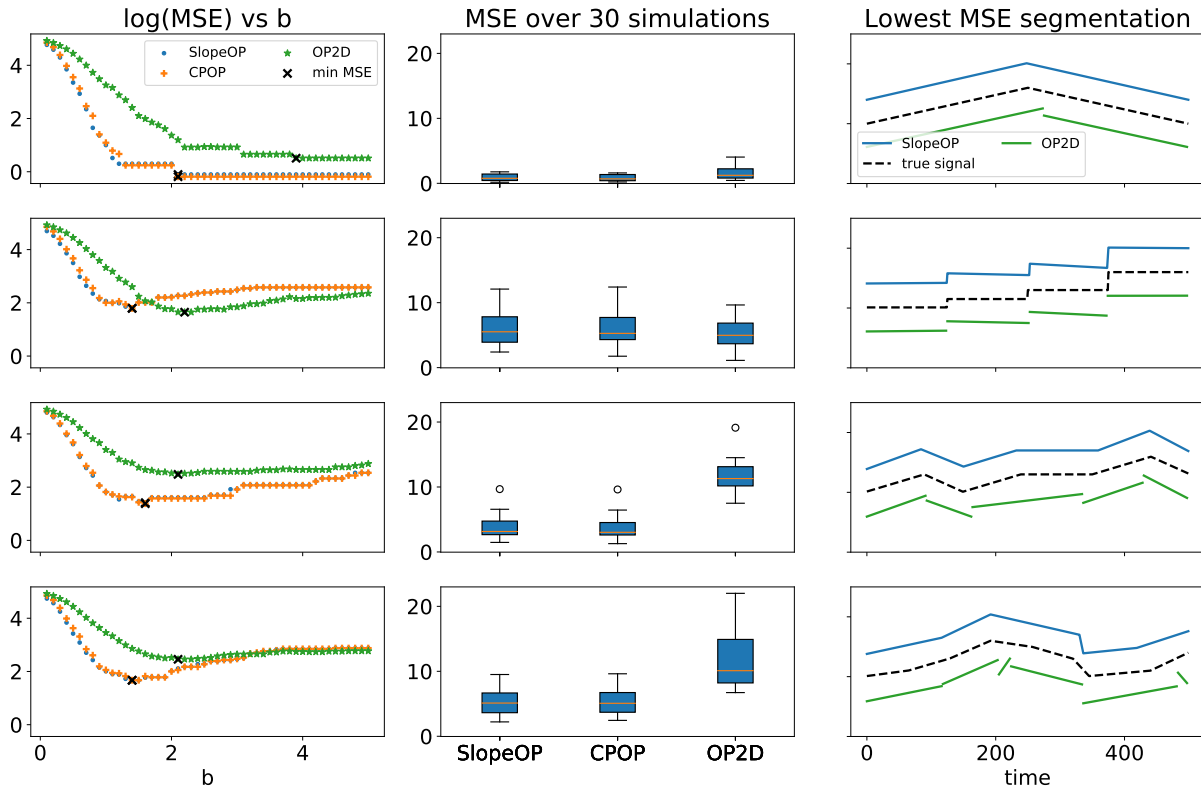


Figure 4: Results for scenarios 1 to 4 with noise  $\sigma = 12$ . Each point of the MSE curve is the mean over 30 independent simulations. For the smallest MSE in each of the 12 MSE curves, we present the 30 corresponding results in the boxplots. The last column shows the obtained segments for the best of the 30 results in boxplots for OP-2D and *slopeOP*.

simulations.

Results show that the MSE as well as the number of segments is lower, whatever the penalty value. With a misspecified model or in presence of outliers, the minimum angle option (when we expect no small angle) improves the result of *slopeOP*. The penalty value has a reduced impact on the algorithm, which can be important for applications when the time series to analysis does not have a Gaussian noise structure.

## 6 Application to Antibigram Image Analysis

Antibiotic Susceptibility Testing (AST) is a microbiology test used to guide antibiotic prescription in bacterial diseases by determining the susceptibility of bacteria to different antibiotics.

In disk diffusion AST, or antibiogram, cellulose disks impregnated with specific antibiotics are placed on the surface of Petri-dishes previously inoculated with a microorganism. Agar plates are incubated so that bacteria can grow everywhere, except around the cellulose disks that contain antibiotics to which the bacteria are susceptible. Then the diameter of the zone of non-growth (inhibition) surrounding each antibiotic disk is measured and compared to known minimum diameters to determine the susceptibility (the comparison is done with a sensibility of one millimeter)[20]. Diameters can be read by eye with a ruler, but several automatic reading systems exist which process pictures of incubated plates [27, 17].

The inhibition zone boundary is usually clear and easy to measure, but it can sometimes be hazy and fuzzy. In most cases, zone edges should be read at the point of complete inhibition[1],

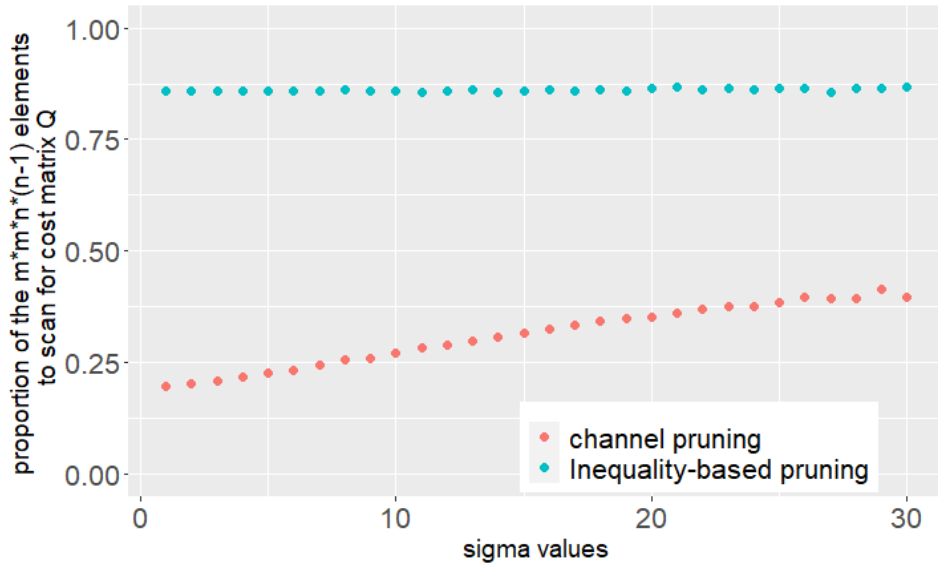


Figure 5: Without pruning the dynamic programming algorithm needs to scan  $m^2n(n-1)$  elements for finding minima at each step. We compare the proportion of elements that the algorithm scans for channel-based and inequality-based prunings with a hat-shaped signal with different noise levels. For all noise levels, the channel method is much more efficient.

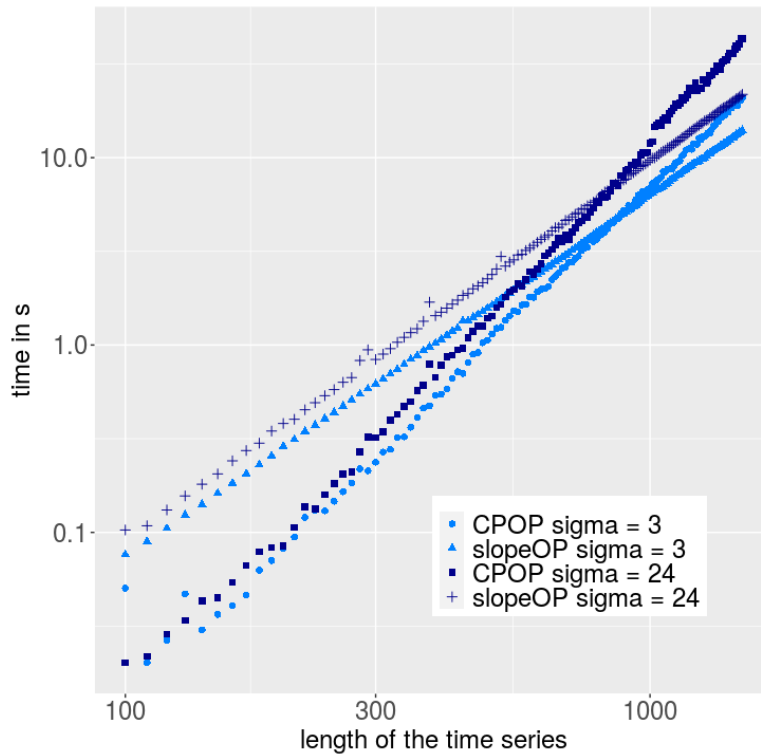


Figure 6: Computational time of CPOP versus *slopeOP* for hat-shaped data with noise level  $\sigma = 3$  and  $\sigma = 24$  in log-log scale. The coefficient  $q$  in complexity  $O(n^q)$  is equal to 2.68 and 2.97 for CPOP for  $\sigma = 3$  and  $\sigma = 24$ , respectively. For *slopeOP* we get 1.93 and 2.01 with the channel pruning option.

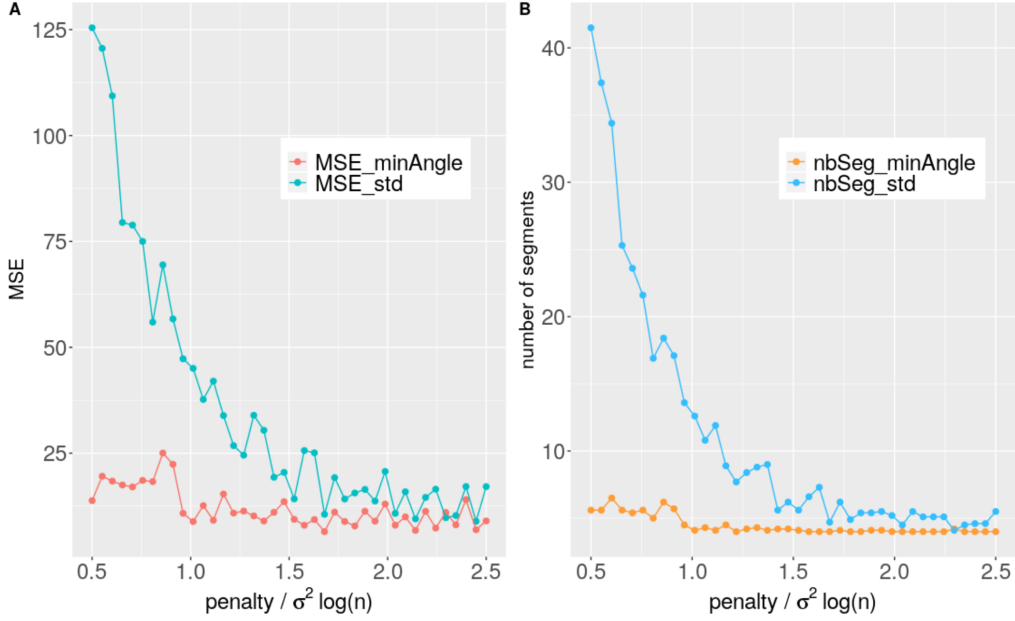


Figure 7: For a range of penalties from  $\beta = 0.5\sigma^2 \log(n)$  to  $\beta = 2.5\sigma^2 \log(n)$ , 10 hat-shaped time series have been simulated with  $n = 500$  for each penalty value and we ran *slopeOP* with a smoothing option ( $minAngle = 130$ ) and without constraint (*std*). On the left panel A, we compare the MSE between the inferred signal and the true one for the two methods; on the right panel B, we compare the number of inferred segments for the two methods. Results highlight the stability with respect to the penalty of the algorithm with minimal angle option.

but determining this point can be challenging.

Several image processing procedures have been proposed for measuring inhibition diameters [13, 11, 6], but none of them focuses specifically on the issue of fuzzy borders. We propose the use of *slopeOP* to measure inhibition diameters in these cases. To our knowledge, a MSE-minimizing optimal segmentation algorithm has never been used to measure AST's inhibition diameters.

We designed a processing pipeline that uses *slopeOP* to read inhibition diameters from the picture of an AST and tested it on one hundred inhibition zones presenting fuzzy borders. Fifty inhibition zones were taken from standard Mueller-Hinton growth medium antibiograms, the other fifty from blood agar antibiograms, which are darker and less contrasted. After normalizing the intensity of the AST picture, a sub-region of each inhibition zone was selected and centered on the antibiotic disk. Then the radial intensity profile  $I(r)$  was extracted: we recorded  $I$ , the average intensity value of the 10 most intense pixels (the scale of the images is  $\simeq 10 \frac{pixel}{mm}$ ) lying at fixed distance  $r$  from the sub-region center (see figure 8). This method is a simple way to detect bacteria even if the inhibition zone is not a perfect disk. The average profile size in the data-set is 230 point.

*slopeOP* was used to segment the radial profile and determine the inhibition zone radius. For the segmentation with *slopeOP* we take the signal starting at 3.5mm, i.e. just after the plateau corresponding to the pellet disk (from this point, the ideal signal is supposed to be isotonic).

*slopeOP* is used with  $\mathcal{S} = \{I(r)_{min}, \dots, I(r)_{max}\}$  and  $\beta = 255$  (the max gray value of a 8-bit image). We tested both with and without the isotonic constraint (as the observed signal is supposed to be isotonic).

After the segmentation, we measure the inhibition radius  $r_{inib}$  as the distance corresponding to the first change-point. The inhibition diameter is obtained as  $d_{inhib} = 2 \times r_{inhib}$ .

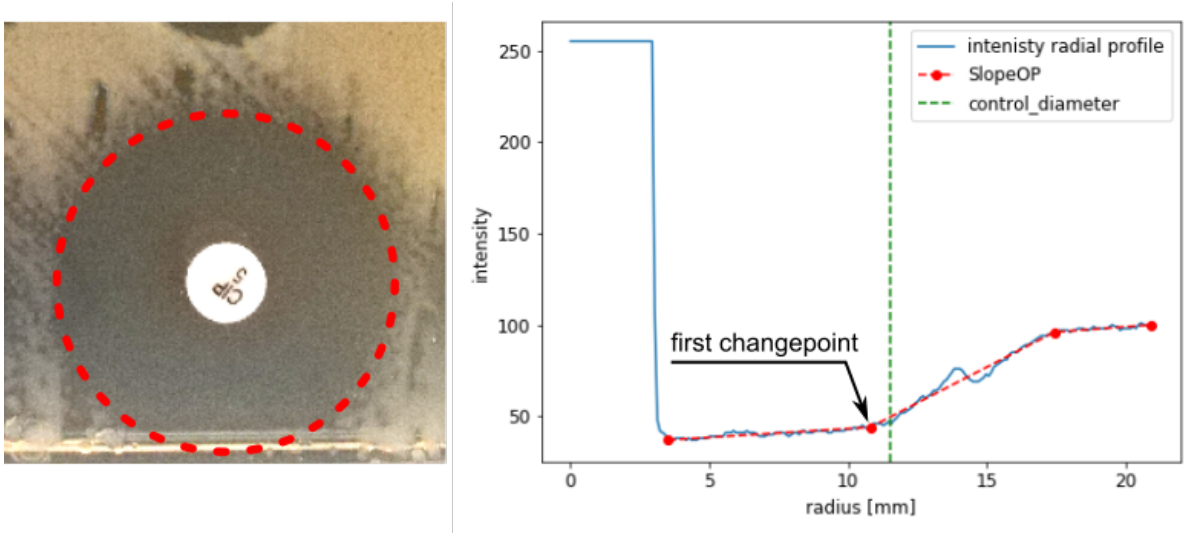


Figure 8: Picture of a part of an antibiogram showing an antibiotic disk and its inhibition zone (left). On the right a plot of the intensity radial profile and the segmentation with *slopeOP* with isotonic constraint.

AST type	algorithm	diameter diff quantiles		
		25%	50%	75%
M-H	slopeOP	0.29	0.91	2.92
	slopeOP-iso	0.24	0.69	1.71
	t-test	0.50	1.50	3.25
blood	slopeOP	0.72	1.72	3.00
	slopeOP-iso	0.47	1.28	2.38
	t-test	2.00	9.50	16.75

Table 2: Agreement of auto and manual reading. We observe the distribution of  $\Delta d = |d_a - d_c|$  the absolute difference between the automatically measured diameter  $d_a$  and the control value  $d_c$ .

As a comparison, we measured the diameters with the method suggested by Gavaille et al.[11] which uses a student t-test thus considering both the intensity and the texture of the pixels around the antibiotic disk.

The so measured diameters were compared with manual (by eye) measurements, by calculating the absolute difference.

The results (Table 2) show a good consistency with the manual measurements. In the case of Mueller-Hinton antibiograms, half of the diameter differences between our procedure and control are below the test sensibility (1mm) and 75% are smaller than 1.5mm, which is comparable with the acknowledged inter-operator variability due to the subjectivity of the measurement ( $\pm 1\text{mm}$ ) [16]. The results on the blood agar ASTs are slightly worse because of the lower contrast in the images and a consequent decreased signal-noise ratio. In both cases the isotonic constraint yields improved results.

Successively we tested the performance of *slopeOP* with isotonic constraint when reducing the density of states by 2,4 and 8. We defined the states space as  $\mathcal{S} = \{I_{min}, I_{min} + s, I_{min} + 2s, \dots, I_{max}\}$  and repeated the measurements on the data-set at each value of  $s = 2, 4, 8$ . The results are reported in Table 3 and show a neat improvement in the execution speed by reducing the states density. Although the precision of the measurement decreases with decreasing states

agar	state density	diameter diff quantiles			speed	mean number of changepoints
		25%	50%	75%		
M-H	1	0.24	0.69	1.71	1.00	4.25
	1/2	0.19	0.64	1.84	2.97	4.33
	1/4	0.21	0.77	1.55	7.74	4.24
	1/8	0.38	0.83	2.57	17.92	4.25
blood	1	0.47	1.28	2.38	1.00	3.92
	1/2	0.43	1.04	1.84	2.76	3.90
	1/4	0.70	1.52	2.34	6.69	3.94
	1/8	1.07	2.05	3.83	14.53	3.96

Table 3: Performance of slopeOP-isotonic at various states density. The calculation speed is reported as the inverse of the average execution time (normalized to density=1). Changepoints=average number of changepoints found. NOTE: Mean execution time for slopeOP-iso1 is 5ms @ 2,3 GHz Intel Core i5.

density, the measured diameter are still in reasonable accord with the control values.

## Acknowledgement

We thank Guillem Rigail (LaMME Evry, IPS2 Paris-Saclay) for joint mentoring of our intern (co-author Nicolas Deschamps de Boishebert), for the carefull reading of this work and the many usefull feedback.

## A Simulation Results for the 4 Scenarios

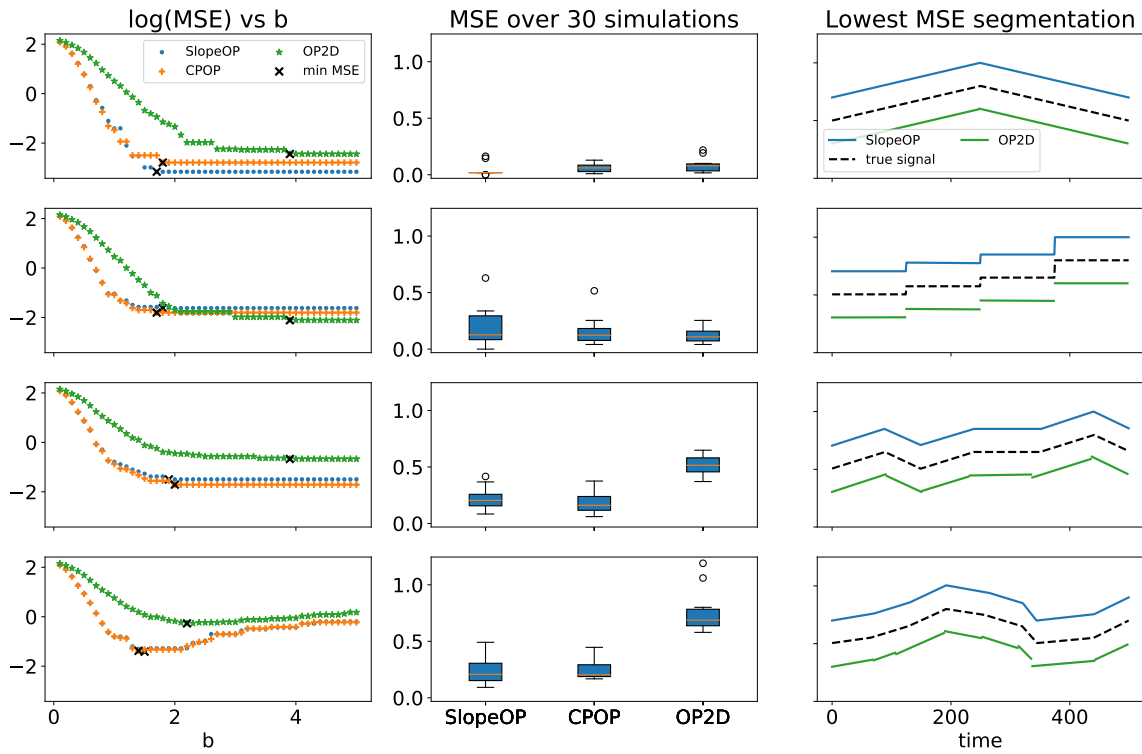


Figure 9: Results for scenarios 1 to 4 with noise  $\sigma = 3$

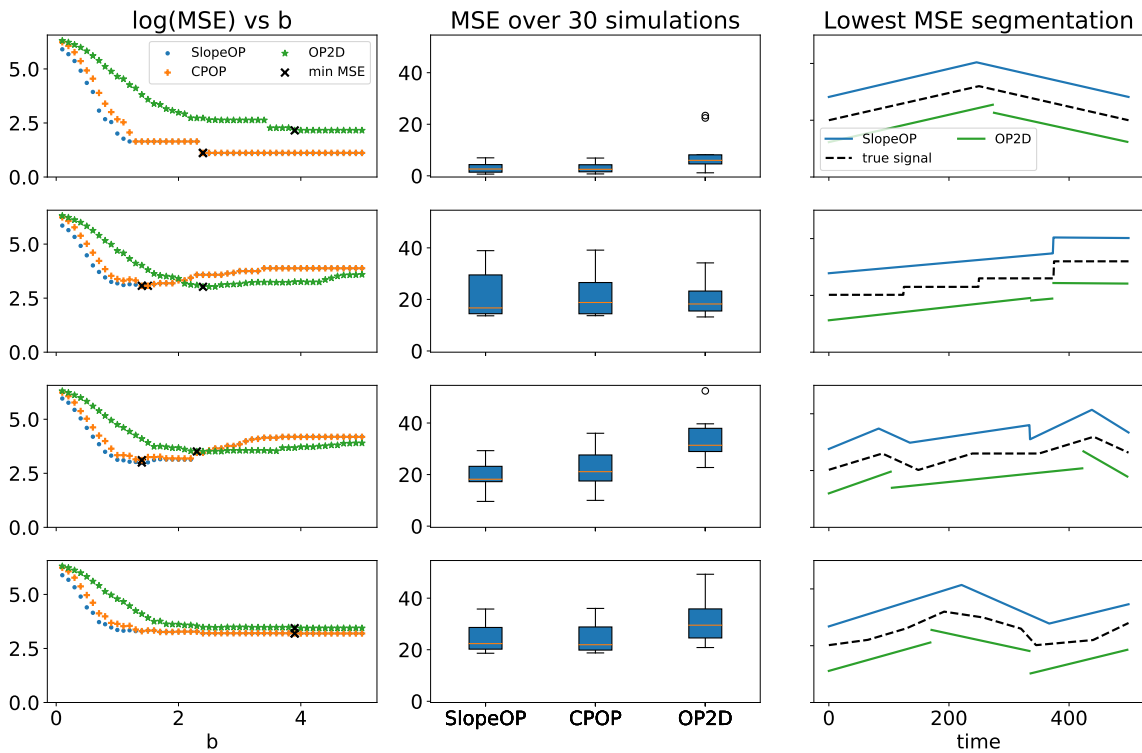


Figure 10: Results for scenarios 1 to 4 with noise  $\sigma = 24$

## References

- [1] Reading guide - eucast disk diffusion method for antimicrobial susceptibility testing. page 3. EUCAST, 2020.
- [2] R. Baranowski, Y. Chen, and P. Fryzlewicz. Narrowest-over-threshold detection of multiple change points and change-point-like features. *Journal of the Royal Statistical Society: Series B (Statistical Methodology)*, 81(3):649–672, 2019.
- [3] C. Beaulieu, J. Chen, and J. L. Sarmiento. Change-point analysis as a tool to detect abrupt climate variations. *Philosophical Transactions of the Royal Society A: Mathematical, Physical and Engineering Sciences*, 370(1962):1228–1249, 2012.
- [4] R. E. Bellman and S. Dreyfus. Applied dynamic programming, princeton unlv. *Press, Princeton, NJ*, 1962.
- [5] H. Cao and W. Biao Wu. Changepoint estimation: another look at multiple testing problems. *Biometrika*, 102(4):974–980, 2015.
- [6] L. F. Costa, E. S. da Silva, V. T. Noronha, I. Vaz-Moreira, O. C. Nunes, and M. M. de Andrade. Development of an automatic identification algorithm for antibiogram analysis. *Computers in biology and medicine*, 67:104–115, 2015.
- [7] I. Cribben and Y. Yu. Estimating whole-brain dynamics by using spectral clustering. *Journal of the Royal Statistical Society: Series C (Applied Statistics)*, 66(3):607–627, 2017.
- [8] P. Fearnhead, R. Maidstone, and A. Letchford. Detecting changes in slope with an l0 penalty. *Journal of Computational and Graphical Statistics*, pages 1–11, 2018.
- [9] P. Fearnhead and G. Rigai. Relating and comparing methods for detecting changes in mean. *Stat*, page e291.
- [10] P. Fearnhead and G. Rigai. Changepoint detection in the presence of outliers. *Journal of the American Statistical Association*, 9 2017.
- [11] A. Gavaille, B. Bardy, and A. Andremont. Measurement of inhibition zone diameter in disk susceptibility tests by computerized image analysis. *Computers in biology and medicine*, 24(3):179–188, 1994.
- [12] P. Hall, J. Kay, and D. Titterinton. Asymptotically optimal difference-based estimation of variance in nonparametric regression. *Biometrika*, 77(3):521–528, 1990.
- [13] G. Hejblum, V. Jarlier, J. Grosset, and A. Aurengo. Automated interpretation of disk diffusion antibiotic susceptibility tests with the radial profile analysis algorithm. *Journal of clinical microbiology*, 31(9):2396–2401, 1993.
- [14] T. Hocking, G. Rigai, and G. Bourque. Peakseg: constrained optimal segmentation and supervised penalty learning for peak detection in count data. In *International Conference on Machine Learning*, pages 324–332, 2015.
- [15] T. D. Hocking, G. Rigai, P. Fearnhead, and G. Bourque. A log-linear time algorithm for constrained changepoint detection. *arXiv preprint arXiv:1703.03352*, 2017.

- [16] M. Hombach, F. P. Maurer, T. Pfiffner, E. C. Böttger, and R. Furrer. Standardization of operator-dependent variables affecting precision and accuracy of the disk diffusion method for antibiotic susceptibility testing. *Journal of clinical microbiology*, 53(12):3864–3869, 2015.
- [17] M. Hombach, R. Zbinden, and E. C. Böttger. Standardisation of disk diffusion results for antibiotic susceptibility testing using the sirscan automated zone reader. *BMC microbiology*, 13(1):225, 2013.
- [18] B. Jackson, J. D. Scargle, D. Barnes, S. Arabhi, A. Alt, P. Gioumouisis, E. Gwin, P. Sangtrakulcharoen, L. Tan, and T. T. Tsai. An algorithm for optimal partitioning of data on an interval. *IEEE Signal Processing Letters*, 12(2):105–108, 2005.
- [19] S. Jamali, P. Jönsson, L. Eklundh, J. Ardö, and J. Seaquist. Detecting changes in vegetation trends using time series segmentation. *Remote Sensing of Environment*, 156:182–195, 2015.
- [20] J. H. Jorgensen and J. D. Turnidge. Susceptibility test methods: Dilution and disk diffusion methods\*. In *Manual of Clinical Microbiology, Eleventh Edition*, pages 1253–1273. American Society of Microbiology, 2015.
- [21] R. Killick, P. Fearnhead, and I. A. Eckley. Optimal detection of changepoints with a linear computational cost. *Journal of the American Statistical Association*, 107(500):1590–1598, 2012.
- [22] L. Koepcke, G. Ashida, and J. Kretzberg. Single and multiple change point detection in spike trains: comparison of different cusum methods. *Frontiers in systems neuroscience*, 10:51, 2016.
- [23] R. Maidstone, T. Hocking, G. Rigaiil, and P. Fearnhead. On optimal multiple changepoint algorithms for large data. *Statistics and Computing*, 27(2):519–533, Mar 2017.
- [24] National Research Council. *Frontiers in massive data analysis*, 2013.
- [25] E. S. Page. Continuous inspection schemes. *Biometrika*, 41(1/2):100–115, 1954.
- [26] G. Rigaiil. A pruned dynamic programming algorithm to recover the best segmentations with 1 to k\_max change-points. *Journal de la Société Française de Statistique*, 156(4):180–205, 2015.
- [27] M. Sanchez, B. S. Del Saz, E. Loza, F. Baquero, and R. Canton. Evaluation of the osiris video reader system for disk diffusion susceptibility test reading. *Clinical microbiology and infection*, 7(7):352–357, 2001.
- [28] A. J. Scott and M. Knott. A cluster analysis method for grouping means in the analysis of variance. *Biometrics*, 30(3):507–512, 1974.
- [29] A. Sen and M. S. Srivastava. On tests for detecting change in mean. *The Annals of statistics*, pages 98–108, 1975.
- [30] Y. Sowa, A. D. Rowe, M. C. Leake, T. Yakushi, M. Homma, A. Ishijima, and R. M. Berry. Direct observation of steps in rotation of the bacterial flagellar motor. *Nature*, 437(7060):916, 2005.

- [31] S. Tickle, I. Eckley, P. Fearnhead, and K. Haynes. Parallelization of a common changepoint detection method. *Journal of Computational and Graphical Statistics*, 29(1):149–161, 2020.
- [32] R. Todd Ogden and G. L. Collier. On detecting and modeling deterministic drift in long run sequences of tapping data. *Communications in Statistics-Theory and Methods*, 28(3-4):977–987, 1999.
- [33] C. Truong, L. Oudre, and N. Vayatis. Selective review of offline change point detection methods. *Signal Processing*, 167:107299, 2020.
- [34] Y.-C. Yao. Estimating the number of change-points via schwarz’criterion. *Statistics & Probability Letters*, 6(3):181–189, 1988.
- [35] M. Yu and E. Ruggieri. Change point analysis of global temperature records. *International Journal of Climatology*, 39(8):3679–3688, 2019.
- [36] C. Zheng, I. A. Eckley, and P. Fearnhead. Consistency of a range of penalised cost approaches for detecting multiple changepoints. *arXiv preprint arXiv:1911.01716*, 2019.